NANOSYSTEMS: PHYSICS, CHEMISTRY, MATHEMATICS, 2014, 5 (5), P. 626–643

# PHOTONIC CRYSTAL WITH NEGATIVE INDEX MATERIAL LAYERS

K. V. Pravdin, I. Yu. Popov

ITMO University, Saint Petersburg, Russia

construeman@gmail.com, popov1955@gmail.com

**PACS 42.70.Qs, 78.67.Pt**

We consider the one-dimensional photonic crystal composed of an infinite number of parallel alternating layers filled with a metamaterial and vacuum. We assume the metamaterial is an isotropic, homogeneous, dispersive and non-absorptive medium. We use a single Lorentz contribution and assume the permittivity and permeability are equal. Using the time and coordinate Fourier transforms and the Floquet-Bloch theorem, we obtain systems of equations for TE and TM modes, which ones are identical. We consider radiative and evanescent regimes for the metamaterial and vacuum layers and find sets of frequencies, where the metamaterial has the positive or negative refractive index. We use a numerical approach. As a result, we obtained the photonic band gap structure for different frequency intervals and ascertain how it changes with modification of the system parameters. We observe the non-reflection effect for any directions for a certain frequency but this fails with the layer width modification.

**Keywords:** phonic crystals, photonic band gap, negative index materials, metamaterial.

*Received: 10 June 2014*
*Revised: 08 July 2014*

## 1. Introduction

Materials with a periodically modulated refractive index function of spatial coordinates are known as photonic crystals (PCs). Photonic crystals occur in nature over millions years. Biological systems were using nanometer-scale architectures, which are the natural photonic structures, to produce striking optical effects [1].

Extensive studies on PCs began with these pioneering works [2, 3]. The propagation of electromagnetic (EM) wave in the PC depends on its frequency and can be forbidden. The forbidden frequencies make up the forbidden bands or so-called photonic band gaps (PBGs). Analogously, the permitted frequencies make up the permitted bands [4, 5]. Forbidden and permitted bands comprise the so-called PBG structure. The PBGs lead to various applications of PCs such as perfect dielectric mirror [6], nonlinear effects [7], resonant cavities [8], PC fibers [9], waveguides [10], and PC devices, e.g., ultra-fast, efficient and high power nanocavity lasers, optical buffer and storage components [11].

The simplest model of a PC is the one-dimensional PC (1DPC). The 1DPC is a system of alternating layers with different refractive indices. Using negative index materials (NIMs) [12, 13] in 1DPCs can lead to unusual phenomena, such as spurious modes with complex frequencies, discrete modes and photon tunneling modes [14]. Therefore, numerous investigations of 1DPC composed of layers filled with positive index materials (PIMs) and NIMs, have been performed recently [15-21]. But, most of these investigations consider nondisperdive systems, i.e., the permittivity and permeability (and therefore, the refractive index) are the same for all frequencies of EM waves.

The goal of our work is to obtain the PBG structure for a system of alternating layers filled with a metamaterial and vacuum. We assume the metamaterial is an isotropic, homogeneous, dispersive and non-absorptive medium. We also assume the permittivity and permeability have the identical expression. We use a single Lorentz contribution to describe them [22, 23]. Therefore, for a certain frequency interval, the metamaterial has a negative refractive index and behaves like a NIM (NIM case). For other frequencies, it has a positive refractive index and behaves like a PIM (PIM case). We have a chance to compare the NIM case with the PIM case. Also, we are interested in the dependence of the PBG structure upon the system's parameters.

## 2. Model

### 2.1. Maxwell's equations

We consider the Maxwell's equations in a differential form:

$$\frac{d\mathbf{D}}{dt}(\mathbf{x},t) = \nabla \times \mathbf{H}(\mathbf{x},t), \tag{1}$$

$$\frac{d\mathbf{B}}{dt}(\mathbf{x},t) = -\nabla \times \mathbf{E}(\mathbf{x},t), \tag{2}$$

$$\nabla \cdot \mathbf{D}(\mathbf{x},t) = 0, \tag{3}$$

$$\nabla \cdot \mathbf{B}(\mathbf{x},t) = 0, \tag{4}$$

where $\mathbf{x}$ is the vector located in the $\{\mathbf{e}_i\}_{i=1}^3$ Cartesian basis, $\nabla$ is the Hamilton operator, $\times$ is a cross product symbol, $\cdot$ is an inner product symbol as well as a symbol for the matrix product. Also, we consider the auxiliary field equations:

$$\mathbf{D}(\mathbf{x},t) = \varepsilon_0 \mathbf{E}(\mathbf{x},t) + \mathbf{P}(\mathbf{x},t), \tag{5}$$

$$\mathbf{B}(\mathbf{x},t) = \mu_0 \left[\mathbf{H}(\mathbf{x},t) + \mathbf{M}(\mathbf{x},t)\right], \tag{6}$$

where

$$\mathbf{P}(\mathbf{x},t) = \varepsilon_0 \int_{t_0}^{t} \boldsymbol{\chi}_e(\mathbf{x},t-s)\cdot \mathbf{E}(\mathbf{x},s)\,ds,$$

$$\mathbf{M}(\mathbf{x},t) = \int_{t_0}^{t} \boldsymbol{\chi}_m(\mathbf{x},t-s)\cdot \mathbf{H}(\mathbf{x},s)\,ds,$$

and $\varepsilon_0$ and $\mu_0$ are the electric and magnetic constants ($\varepsilon_0\mu_0 = 1/c^2$, where $c$ is the speed of light in vacuum), $\boldsymbol{\chi}_e(\mathbf{x},t)$ and $\boldsymbol{\chi}_m(\mathbf{x},t)$ are the electric and magnetic susceptibility tensors. We use the causality condition $\boldsymbol{\chi}_e(\mathbf{x},t) = \boldsymbol{\chi}_m(\mathbf{x},t) = 0$ for $t < t_0$ and assume $t_0 = 0$. We also use the passivity condition [23]. Then, the electromagnetic energy,

$$U_{em}(t) = \frac{1}{2}\int \left[\mathbf{E}^2(\mathbf{x},t) + \mathbf{H}^2(\mathbf{x},t)\right] d\mathbf{x},$$

is a non-increasing function of time. With the causality and passivity conditions and the auxiliary field formalism (AFF), the system has a proper time evolution [23]. In case the initial fields are square integrable they remain so for all later times.

We use the Fourier transform with $t$ time,

$$\hat{f}(\omega) = \int_{-\infty}^{+\infty} f(t)\, e^{-i\omega t} dt, \quad f(t) = \frac{1}{2\pi}\int_{-\infty}^{+\infty} \hat{f}(\omega)\, e^{i\omega t} d\omega, \tag{7}$$

to obtain the Maxwell's equations (1)–(4) in relation on $\omega$ frequency

$$i\omega \hat{\mathbf{D}}(\mathbf{x},\omega) = \nabla \times \hat{\mathbf{H}}(\mathbf{x},\omega), \tag{8}$$

$$i\omega\hat{\mathbf{B}}(\mathbf{x},\omega) = -\nabla\times\hat{\mathbf{E}}(\mathbf{x},\omega), \tag{9}$$

$$\nabla\cdot\hat{\mathbf{D}}(\mathbf{x},\omega) = 0, \tag{10}$$

$$\nabla\cdot\hat{\mathbf{B}}(\mathbf{x},\omega) = 0. \tag{11}$$

The auxiliary field equations (5) and (6) after the Fourier transform (7) are expressed as follows:

$$\hat{\mathbf{D}}(\mathbf{x},\omega) = \varepsilon_0\boldsymbol{\varepsilon}(\mathbf{x},\omega)\cdot\hat{\mathbf{E}}(\mathbf{x},\omega), \tag{12}$$

$$\hat{\mathbf{B}}(\mathbf{x},\omega) = \mu_0\boldsymbol{\mu}(\mathbf{x},\omega)\cdot\hat{\mathbf{H}}(\mathbf{x},\omega), \tag{13}$$

where

$$\boldsymbol{\varepsilon}(\mathbf{x},\omega) = 1 + \hat{\boldsymbol{\chi}}_e(\mathbf{x},\omega),$$
$$\boldsymbol{\mu}(\mathbf{x},\omega) = 1 + \hat{\boldsymbol{\chi}}_m(\mathbf{x},\omega).$$

Substituting expressions for $\hat{\mathbf{D}}(\mathbf{x},\omega)$ and $\hat{\mathbf{B}}(\mathbf{x},\omega)$ from equations (12) and (13) into equations (8), (9), (10), and (11), we obtain the following relations:

$$i\omega\varepsilon_0\boldsymbol{\varepsilon}(\mathbf{x},\omega)\hat{\mathbf{E}}(\mathbf{x},\omega) = \nabla\times\hat{\mathbf{H}}(\mathbf{x},\omega), \tag{14}$$

$$i\omega\mu_0\boldsymbol{\mu}(\mathbf{x},\omega)\hat{\mathbf{H}}(\mathbf{x},\omega) = -\nabla\times\hat{\mathbf{E}}(\mathbf{x},\omega), \tag{15}$$

$$\nabla\cdot\hat{\mathbf{E}}(\mathbf{x},\omega) = 0,$$
$$\nabla\cdot\hat{\mathbf{H}}(\mathbf{x},\omega) = 0.$$

We examine the system composed of infinite count of parallel layers. $\mathbf{e}_1$, $\mathbf{e}_2$ unit vectors set the plane of the layer's surfaces. $\mathbf{e}_3$ unit vector set the $x$ axis. We assume a translation invariance along the plane of layer's surfaces. There are two types of layers. The first one is $\Delta_1$ in width and filled with a metamaterial. The second one is $\Delta_2$ in width and filled with a vacuum. Layers alternate with each other. Then, $\Delta_1+\Delta_2$ is the period of the system. Thus, the system is a 1DPC, and it is enough to consider only two layers, e.g., the metamaterial layer located between $x=0$ and $x=\Delta_1$ coordinates (let its index be $j=1$) and the vacuum layer located between $x=\Delta_1$ and $x=\Delta_1+\Delta_2$ coordinates (let its index be $j=2$).

We assume that the metamaterial layers are isotropic and homogeneous media. Therefore, the permittivity and permeability in all metamaterial layera are scalar functions only of the one $\omega$ frequency variable, i.e., $\boldsymbol{\varepsilon}(\mathbf{x},\omega)=\varepsilon(\omega)\mathbf{U}$ and $\boldsymbol{\mu}(\mathbf{x},\omega)=\mu(\omega)\mathbf{U}$. Also, we assume the metamaterial layers are dispersive and non-absorptive media. In that case, the susceptibilities consist of a sum of Lorentz contributions [22]. We deal with a single dispersive Lorentz contribution [23]. We assume that the permittivity and permeability of the metamaterial stand equal and

$$\varepsilon(\omega) = \mu(\omega) = 1 - \frac{\Omega^2}{\omega^2-\omega_0^2}, \tag{16}$$

where $\Omega$ and $\omega_0$ are constants, and $\varepsilon(\omega)=\mu(\omega)=1$ in vacuum. From equation (16) it follows that for different $\omega$ frequencies the metamaterial behaves like a PIM or NIM (and we have the PIM or NIM system). For every $\omega$ inside the $(\omega_0,\omega_2)$ interval (NIM interval) the $\varepsilon(\omega)$ and $\mu(\omega)$ values are negative and the metamaterial is the NIM, where $\omega_2=\sqrt{\omega_0^2+\Omega^2}$, $\varepsilon(\omega_2)=\mu(\omega_2)=0$, and $\varepsilon(\omega_0+0)=\mu(\omega_0+0)=-\infty$. For every $\omega$ inside the $(0,\omega_0)$ or $(\omega_2,+\infty)$ intervals (first and second PIM interval, correspondingly) the $\varepsilon(\omega)$ and $\mu(\omega)$ values are positive and the metamaterial is the PIM, where $\varepsilon(\omega_0-0)=\mu(\omega_0-0)=+\infty$. For $\omega_1=\sqrt{\omega_0^2+\Omega^2/2}$ in the metamaterial $\varepsilon(\omega_1)=\mu(\omega_1)=-1$, where $\omega_1$ is so-called NIM frequency [23].

Expressing the $\hat{\mathbf{H}}(\mathbf{x},\omega)$ value from equation (15), substituting it into equation (14) and recalling $\varepsilon_0\mu_0 = 1/c^2$, we obtain the Helmholtz equation for $j$-th layer ($j = 1, 2$) as follows:

$$\nabla \times \nabla \times\, \hat{\mathbf{E}}_j(\mathbf{x},\omega) = (\omega/c)^2\varepsilon_j(\omega)\mu_j(\omega)\hat{\mathbf{E}}_j(\mathbf{x},\omega). \tag{17}$$

Let $\mathbf{k} = \{k_1, k_2, k_3\}$ be a three-dimensional wave vector with $k$ length, where $k = k(\omega) = (\omega/c)^2\varepsilon(\omega)\mu(\omega)$, $\boldsymbol{\kappa} = \{k_1, k_2, 0\} = \kappa\mathbf{e}_{\boldsymbol{\kappa}}$ be a two-dimensional wave vector with $\kappa$ coordinate along the $\mathbf{e}_{\boldsymbol{\kappa}}$ unit vector, which is parallel to the plane of layer's surfaces, $\boldsymbol{\zeta} = \{0, 0, k_3\} = \zeta\mathbf{e}_3$ is an one-dimensional wave vector parallel to the $x$ axis with the $\zeta$ coordinate, where $\zeta^2 = \zeta^2(\omega,\kappa) = k^2(\omega) - \kappa^2 = (\omega/c)^2\varepsilon(\omega)\mu(\omega) - \kappa^2$. Therefore, $\mathbf{e}_3 \times \mathbf{e}_{\boldsymbol{\kappa}}$ is a parallel to the plane of layer's surfaces unit vector. The set of $\mathbf{e}_{\boldsymbol{\kappa}}$, $\mathbf{e}_3 \times \mathbf{e}_{\boldsymbol{\kappa}}$, $\mathbf{e}_3$ unit vectors forms the Cartesian basis.

The considered system is the 1DPC. Then, to obtain the following one-dimensional expression of the Helmholtz equation (17), we use the Fourier transform with $x_1$ and $x_2$ coordinates of $\mathbf{x}^\perp = \{x_1, x_2, 0\}$ vector:

$$g_{\boldsymbol{\kappa}}(x) = \int_{-\infty}^{+\infty}\int_{-\infty}^{+\infty} e^{i(k_1x_1+k_2x_2)} g(\mathbf{x})dx_1dx_2 = \int_{\mathrm{R}^2} e^{i\boldsymbol{\kappa}\cdot\mathbf{x}^\perp} g(\mathbf{x})d\mathbf{x}^\perp, \tag{18}$$

$$g(\mathbf{x}) = \frac{1}{(2\pi)^2}\int_{-\infty}^{+\infty}\int_{-\infty}^{+\infty} e^{-i(k_1x_1+k_2x_2)} g_{\boldsymbol{\kappa}}(x)dk_1dk_2 = \frac{1}{(2\pi)^2}\int_{\mathrm{R}^2} e^{-i\boldsymbol{\kappa}\cdot\mathbf{x}^\perp} g_{\boldsymbol{\kappa}}(x)d\boldsymbol{\kappa}.$$

The Fourier transformed (18) Hamilton operator is

$$\nabla_{\boldsymbol{\kappa}} = \left(i\boldsymbol{\kappa} + \frac{\partial}{\partial x_3}\mathbf{e}_3\right).$$

Then,

$$\left[\nabla \times \nabla \times\, \hat{\mathbf{E}}_j(\mathbf{x},\omega)\right]_{\boldsymbol{\kappa}} = \left(i\boldsymbol{\kappa} + \frac{\partial}{\partial x_3}\mathbf{e}_3\right) \times \left[\left(i\boldsymbol{\kappa} + \frac{\partial}{\partial x_3}\mathbf{e}_3\right) \times \hat{\mathbf{E}}_{\boldsymbol{\kappa},j}(x,\omega)\right],$$

and the Fourier transformed Helmholtz equation (17) is expressed as follows:

$$\left(i\boldsymbol{\kappa} + \frac{\partial}{\partial x_3}\mathbf{e}_3\right) \times \left[\left(i\boldsymbol{\kappa} + \frac{\partial}{\partial x_3}\mathbf{e}_3\right) \times \hat{\mathbf{E}}_{\boldsymbol{\kappa},j}(x,\omega)\right] = (\omega/c)^2\varepsilon_j(\omega)\mu_j(\omega)\hat{\mathbf{E}}_{\boldsymbol{\kappa},j}(x,\omega),$$

or in a matrix form:

$$\mathbf{M}_{\boldsymbol{\kappa},j}(\omega,\kappa)\cdot\hat{\mathbf{E}}_{\boldsymbol{\kappa},j}(x,\omega) = 0, \tag{19}$$

where

$$\mathbf{M}_{\boldsymbol{\kappa},j}(\omega,\kappa) = \begin{pmatrix} \frac{\partial^2}{\partial x^2} + (\omega/c)^2\varepsilon_j(\omega)\mu_j(\omega) & 0 & -i\kappa\frac{\partial}{\partial x} \\ 0 & \frac{\partial^2}{\partial x^2} + \zeta_j^2(\omega,\kappa) & 0 \\ -i\kappa\frac{\partial}{\partial x} & 0 & \zeta_j^2(\omega,\kappa) \end{pmatrix}$$

is presented in $\{\mathbf{e}_{\boldsymbol{\kappa}}, \mathbf{e}_3 \times \mathbf{e}_{\boldsymbol{\kappa}}, \mathbf{e}_3\}$ basis. Equation (19) has the following TE part:

$$\left(\frac{\partial^2}{\partial x^2} + \zeta_j^2(\omega,\kappa)\right)\hat{\mathbf{E}}_{\boldsymbol{\kappa},j}(x,\omega)\Big|_{\mathbf{e}_3\times\mathbf{e}_{\boldsymbol{\kappa}}} = 0, \tag{20}$$

and the following TM part:

$$\left(\frac{\partial^2}{\partial x^2} + (\omega/c)^2\varepsilon_j(\omega)\mu_j(\omega)\right)\hat{\mathbf{E}}_{\boldsymbol{\kappa},j}(x,\omega)\Big|_{\mathbf{e}_{\boldsymbol{\kappa}}} = i\kappa\frac{\partial}{\partial x}\,\hat{\mathbf{E}}_{\boldsymbol{\kappa},j}(x,\omega)\Big|_{\mathbf{e}_3}, \tag{21}$$

$$i\kappa\frac{\partial}{\partial x}\,\hat{\mathbf{E}}_{\boldsymbol{\kappa},j}(x,\omega)\Big|_{\mathbf{e}_{\boldsymbol{\kappa}}} = \zeta_j^2\,\hat{\mathbf{E}}_{\boldsymbol{\kappa},j}(x,\omega)\Big|_{\mathbf{e}_3}, \tag{22}$$

where for a certain $\mathbf{A}$ vector, $\mathbf{A}\big|_{\mathbf{e}}$ notation means its projection on the $\mathbf{e}$ unit vector. Equations (21) and (22) are expressed as follows:

$$\left(\frac{\partial^2}{\partial x^2} + \zeta_j^2(\omega,\kappa)\right) \hat{\mathbf{E}}_{\boldsymbol{\kappa},j}(x,\omega)\Big|_{\mathbf{e}_{\boldsymbol{\kappa}}} = 0, \tag{23}$$

$$\hat{\mathbf{E}}_{\boldsymbol{\kappa},j}(x,\omega)\Big|_{\mathbf{e}_3} = i\kappa \frac{1}{\zeta_j^2(\omega,\kappa)} \frac{\partial}{\partial x} \hat{\mathbf{E}}_{\boldsymbol{\kappa},j}(x,\omega)\Big|_{\mathbf{e}_{\boldsymbol{\kappa}}}. \tag{24}$$

To obtain the $\hat{\mathbf{E}}_{\boldsymbol{\kappa},j}(x,\omega)$ value, it is enough to solve equations (20) and (23) and use equation (24). Equations (20) and (23) have the same structure and can be written as follows:

$$\left(\frac{\partial^2}{\partial x^2} + \zeta_j^2(\omega,\kappa)\right) E_j(x,\omega) = 0, \tag{25}$$

where $E_j(x,\omega) = \hat{\mathbf{E}}_{\boldsymbol{\kappa},j}(x,\omega)\Big|_{\mathbf{e}_3\times\mathbf{e}_{\boldsymbol{\kappa}}}$ for TE mode or $E_j(x,\omega) = \hat{\mathbf{E}}_{\boldsymbol{\kappa},j}(x,\omega)\Big|_{\mathbf{e}_{\boldsymbol{\kappa}}}$ for TM mode.

### 2.2. Boundary conditions

Layers in the system are divided by plane unbounded surfaces. The general form of standard boundary conditions for the surface located between considered layers at the $x = \Delta_1$ coordinate, is presented as follows:

$$(\mathbf{E}_1 - \mathbf{E}_2) \times \mathbf{e}_3 = \mathbf{0}, \tag{26}$$

$$(\mathbf{H}_1 - \mathbf{H}_2) \times \mathbf{e}_3 = \mathbf{0}, \tag{27}$$

$$(\mathbf{D}_1 - \mathbf{D}_2) \cdot \mathbf{e}_3 = 0, \tag{28}$$

$$(\mathbf{B}_1 - \mathbf{B}_2) \cdot \mathbf{e}_3 = 0, \tag{29}$$

where $\mathbf{E}_j = \mathbf{E}_j(\tilde{\mathbf{x}},t)$, $\mathbf{H}_j = \mathbf{H}_j(\tilde{\mathbf{x}},t)$, $\mathbf{D}_j = \mathbf{D}_j(\tilde{\mathbf{x}},t)$, and $\mathbf{B}_j = \mathbf{B}_j(\tilde{\mathbf{x}},t)$ stand for the one-sided limits with $x \to \Delta_1$, $\mathbf{x} = \mathbf{x}^\perp + x\mathbf{e}_3$, and $\tilde{\mathbf{x}} = \mathbf{x}^\perp + \Delta_1\mathbf{e}_3$ (left-sided ones are for $j = 1$ and right-sided ones are for $j = 2$). After the Fourier transform (7), equations (26)–(29) are expressed as follows: $x = \Delta_1$

$$\left(\hat{\mathbf{E}}_1(\tilde{\mathbf{x}},\omega) - \hat{\mathbf{E}}_2(\tilde{\mathbf{x}},\omega)\right) \times \mathbf{e}_3 = \mathbf{0}, \tag{30}$$

$$\left(\hat{\mathbf{H}}_1(\tilde{\mathbf{x}},\omega) - \hat{\mathbf{H}}_2(\tilde{\mathbf{x}},\omega)\right) \times \mathbf{e}_3 = \mathbf{0}, \tag{31}$$

$$\left(\varepsilon_1(\omega)\hat{\mathbf{E}}_1(\tilde{\mathbf{x}},\omega) - \varepsilon_2(\omega)\hat{\mathbf{E}}_2(\tilde{\mathbf{x}},\omega)\right) \cdot \mathbf{e}_3 = 0, \tag{32}$$

$$\left(\mu_1(\omega)\hat{\mathbf{H}}_1(\tilde{\mathbf{x}},\omega) - \mu_2(\omega)\hat{\mathbf{H}}_2(\tilde{\mathbf{x}},\omega)\right) \cdot \mathbf{e}_3 = 0.$$

Let us consider the case of TM mode. It is enough to use the following coordinate representation of equations (30) and (32):

$$\left(\hat{\mathbf{E}}_1(\tilde{\mathbf{x}},\omega) - \hat{\mathbf{E}}_2(\tilde{\mathbf{x}},\omega)\right)\Big|_{\mathbf{e}_\kappa} = 0, \tag{33}$$

$$\left(\varepsilon_1(\omega)\hat{\mathbf{E}}_1(\tilde{\mathbf{x}},\omega) - \varepsilon_2(\omega)\hat{\mathbf{E}}_2(\tilde{\mathbf{x}},\omega)\right)\Big|_{\mathbf{e}_3} = 0. \tag{34}$$

After the Fourier transform (18), equations (33) and (34) are expressed as follows:

$$\left(\hat{\mathbf{E}}_{1,\kappa}(\tilde{x},\omega) - \hat{\mathbf{E}}_{2,\kappa}(\tilde{x},\omega)\right)\Big|_{\mathbf{e}_\kappa} = 0,$$

$$\left(\varepsilon_1(\omega)\hat{\mathbf{E}}_{1,\kappa}(\tilde{x},\omega) - \varepsilon_2(\omega)\hat{\mathbf{E}}_{2,\kappa}(\tilde{x},\omega)\right)\Big|_{\mathbf{e}_3} = 0.$$

Recalling $E_j(x,\omega) = \hat{\mathbf{E}}_{\boldsymbol{\kappa},j}(x,\omega)\Big|_{\mathbf{e}_{\boldsymbol{\kappa}}}$ for TM mode and using equation (24), we obtain:

$$E_1(\Delta_1,\omega) = E_2(\Delta_1,\omega), \tag{35}$$

$$\frac{\partial E_1}{\partial x}(\Delta_1,\omega) = \frac{\varepsilon_2(\omega)}{\varepsilon_1(\omega)}\frac{\zeta_1^2(\omega,\kappa)}{\zeta_2^2(\omega,\kappa)}\frac{\partial E_2}{\partial x}(\Delta_1,\omega). \tag{36}$$

Now we consider the case of TE mode. It is enough to use the following coordinate representation of equations (30) and (31):

$$\left(\hat{\mathbf{E}}_1(\tilde{\mathbf{x}},\omega) - \hat{\mathbf{E}}_2(\tilde{\mathbf{x}},\omega)\right)\Big|_{\mathbf{e}_3\times\mathbf{e}_\kappa} = 0, \tag{37}$$

$$\left(\hat{\mathbf{H}}_1(\tilde{\mathbf{x}},\omega) - \hat{\mathbf{H}}_2(\tilde{\mathbf{x}},\omega)\right)\Big|_{\mathbf{e}_\kappa} = 0. \tag{38}$$

From equation (15) we have

$$\hat{\mathbf{H}}_j(\mathbf{x},\omega) = -\frac{1}{i\omega\mu_0\mu_j(\omega)}\nabla\times\hat{\mathbf{E}}_j(\mathbf{x},\omega).$$

Then, equation (38) is expressed as follows:

$$\left(\nabla\times\hat{\mathbf{E}}_1(\mathbf{x},\omega) - \frac{\mu_1(\omega)}{\mu_2(\omega)}\nabla\times\hat{\mathbf{E}}_2(\mathbf{x},\omega)\right)\Bigg|_{\mathbf{e}_\kappa}^{\mathbf{x}=\tilde{\mathbf{x}}} = 0.$$

Projecting on the $\mathbf{e}_{\boldsymbol{\kappa}}$ unit vector and using the fact that $\hat{\mathbf{E}}_j(\mathbf{x},\omega)\Big|_{\mathbf{e}_3} = 0$ for TE mode, we obtain

$$\frac{\partial}{\partial x}\left(\hat{\mathbf{E}}_1(\mathbf{x},\omega) - \frac{\mu_1(\omega)}{\mu_2(\omega)}\hat{\mathbf{E}}_2(\mathbf{x},\omega)\right)\Bigg|_{\mathbf{e}_3\times\mathbf{e}_\kappa}^{\mathbf{x}=\tilde{\mathbf{x}}}. \tag{39}$$

After Fourier transform (18), equations (37) and (39) are expressed as follows:

$$\left(\hat{\mathbf{E}}_{1,\kappa}(\tilde{x},\omega) - \hat{\mathbf{E}}_{2,\kappa}(\tilde{x},\omega)\right)\Big|_{\mathbf{e}_3\times\mathbf{e}_\kappa} = 0,$$

$$\frac{\partial}{\partial x}\left(\hat{\mathbf{E}}_{1,\kappa}(x,\omega) - \frac{\mu_1(\omega)}{\mu_2(\omega)}\hat{\mathbf{E}}_{2,\kappa}(x,\omega)\right)\Bigg|_{\mathbf{e}_3\times\mathbf{e}_\kappa}^{x=\tilde{x}} = 0,$$

Recalling $E_j(x,\omega) = \hat{\mathbf{E}}_{\kappa,j}(x,\omega)\Big|_{\mathbf{e}_3\times\mathbf{e}_\kappa}$, we obtain:

$$E_1(\Delta_1,\omega) = E_2(\Delta_1,\omega), \tag{40}$$

$$\frac{\partial E_1}{\partial x}(\Delta_1,\omega) = \frac{\mu_1(\omega)}{\mu_2(\omega)}\frac{\partial E_2}{\partial x}(\Delta_1,\omega). \tag{41}$$

Now let us consider the surface located at the $x = \Delta_1 + \Delta_2$ coordinate between the considered vacuum layer ($j = 2$) and the next metamaterial layer (we denote it with the $j = 3$ index). The standard boundary conditions for this surface are presented by equations (26)–(29), where $j = 1$ should be replaced with $j = 3$, $x \to \Delta_1 + \Delta_2$, and the field functions are calculated as left-handed limits for $j = 2$ and right-handed limits for $j = 3$. Analogously to the way we expressed equations (35), (36), (40), and (41) for the surface at the $x = \Delta_1$ coordinate, we obtain the following relations for the surface at the $x = \Delta_1 + \Delta_2$ coordinate for the TM mode:

$$E_3(\Delta_1+\Delta_2,\omega) = E_2(\Delta_1+\Delta_2,\omega), \tag{42}$$

$$\frac{\partial E_3}{\partial x}(\Delta_1+\Delta_2,\omega) = \frac{\varepsilon_2(\omega)}{\varepsilon_3(\omega)}\frac{\zeta_3^2(\omega,\kappa)}{\zeta_2^2(\omega,\kappa)}\frac{\partial E_2}{\partial x}(\Delta_1+\Delta_2,\omega). \tag{43}$$

and for the TE mode:

$$E_3(\Delta_1+\Delta_2,\omega)=E_2(\Delta_1+\Delta_2,\omega), \tag{44}$$

$$\frac{\partial E_3}{\partial x}(\Delta_1+\Delta_2,\omega)=\frac{\mu_3(\omega)}{\mu_2(\omega)}\frac{\partial E_2}{\partial x}(\Delta_1+\Delta_2,\omega). \tag{45}$$

The considered system is periodic. Therefore, $\varepsilon_3(\omega)=\varepsilon_1(\omega)$, $\mu_3(\omega)=\mu_1(\omega)$, $\zeta_3(\omega,\kappa)=\zeta_1(\omega,\kappa)$, and we can use the Floquet-Bloch theorem [24, 25, 26]. This theorem states that if $E$ is a field in a periodic medium with periodicity $\Delta$, then it has to satisfy

$$E(x+\Delta)=e^{i\theta\Delta}E(x),$$

where $\theta$ is a yet undefined wave vector, called the Bloch wave vector. Application of the Floquet-Bloch theorem with $\Delta=\Delta_1+\Delta_2$ leads to the following equations:

$$E_3(\Delta_1+\Delta_2,\omega)=E_1(0,\omega)e^{i\theta(\Delta_1+\Delta_2)},$$

$$\frac{\partial E_3}{\partial x}(\Delta_1+\Delta_2,\omega)=\frac{\partial E_1}{\partial x}(0,\omega)e^{i\theta(\Delta_1+\Delta_2)},$$

where functions with $j=3$ and $j=1$ indices denote left- and right-sided limits respectively. Thus, equations (42) and (43), which correspond to the TM mode, are expressed as follows:

$$E_1(0,\omega)=E_2(\Delta_1+\Delta_2,\omega)e^{-i\theta(\Delta_1+\Delta_2)}, \tag{46}$$

$$\frac{\partial E_1}{\partial x}(0,\omega)=\frac{\varepsilon_2(\omega)}{\varepsilon_1(\omega)}\frac{\zeta_1^2(\omega,\kappa)}{\zeta_2^2(\omega,\kappa)}\frac{\partial E_2}{\partial x}(\Delta_1+\Delta_2,\omega)e^{-i\theta(\Delta_1+\Delta_2)}. \tag{47}$$

Equations (44) and (45), which correspond to the TE mode, are obtained as follows:

$$E_1(0,\omega)=E_2(\Delta_1+\Delta_2,\omega)e^{-i\theta(\Delta_1+\Delta_2)}, \tag{48}$$

$$\frac{\partial E_1}{\partial x}(0,\omega)=\frac{\mu_1(\omega)}{\mu_2(\omega)}\frac{\partial E_2}{\partial x}(\Delta_1+\Delta_2,\omega)e^{-i\theta(\Delta_1+\Delta_2)}. \tag{49}$$

Thus, we have two sets of equations: (35), (36), (46), and (47) for the TM mode and (40), (41), (48), and (49) for the TE mode.

### 2.3. Solutions

Solutions of equation (25) are obtained through the fundamental solution system as follows:

$$E_1(x,\omega)=Ae^{i\zeta_1 x}+Be^{-i\zeta_1 x}, \tag{50}$$

$$E_2(x,\omega)=Ce^{i\zeta_2 x}+De^{-i\zeta_2 x}, \tag{51}$$

where $A$, $B$, $C$, and $D$ are unknown coefficients, $\zeta_j=\zeta_j(\omega,\kappa)$ for $j=1,2$. Using the solutions (50) and (51), we obtain two algebraic systems of equations for the unknown coefficients $A$, $B$, $C$, and $D$. The first one is composed of equations (35), (36), (46), and (47). The second one composed of equations (40), (41), (48), and (49). To solve the first system, we the denote corresponding matrix of the system coefficients in the following manner:

$$K_1(\omega,\kappa)=\begin{pmatrix} e^{i\zeta_1\Delta_1} & e^{-i\zeta_1\Delta_1} & -e^{i\zeta_2\Delta_1} & -e^{-i\zeta_2\Delta_1} \\ e^{i\zeta_1\Delta_1} & -e^{-i\zeta_1\Delta_1} & -\frac{\varepsilon_2}{\varepsilon_1}\frac{\zeta_1}{\zeta_2}e^{i\zeta_2\Delta_1} & \frac{\varepsilon_2}{\varepsilon_1}\frac{\zeta_1}{\zeta_2}e^{-i\zeta_2\Delta_1} \\ 1 & 1 & -e^{i\zeta_2(\Delta_1+\Delta_2)}e^{-i\theta(\Delta_1+\Delta_2)} & -e^{-i\zeta_2(\Delta_1+\Delta_2)}e^{-i\theta(\Delta_1+\Delta_2)} \\ 1 & -1 & -\frac{\varepsilon_2}{\varepsilon_1}\frac{\zeta_1}{\zeta_2}e^{i\zeta_2(\Delta_1+\Delta_2)}e^{-i\theta(\Delta_1+\Delta_2)} & \frac{\varepsilon_2}{\varepsilon_1}\frac{\zeta_1}{\zeta_2}e^{-i\zeta_2(\Delta_1+\Delta_2)}e^{-i\theta(\Delta_1+\Delta_2)} \end{pmatrix},$$

where $\varepsilon_j = \varepsilon_j(\omega)$ and $\zeta_j = \zeta_j(\omega, \kappa)$ for $j = 1, 2$, and compare the det $K_1(\omega, \kappa)$ determinant to zero. Then, we obtain the following relation:

$$\begin{gathered}\left(e^{-i\theta(\Delta_1+\Delta_2)}\right)^2 - \left[\frac{\sigma_{1,2}^{+}\sigma_{2,1}^{+}}{4}\left(1+e^{i2\zeta_1\Delta_1}e^{i2\zeta_2\Delta_2}\right)+\frac{\sigma_{1,2}^{-}\sigma_{2,1}^{-}}{4}\left(e^{i2\zeta_1\Delta_1}+e^{i2\zeta_2\Delta_2}\right)\right]\times \\ \times e^{-i\zeta_1\Delta_1}e^{-i\zeta_2\Delta_2}e^{-i\theta(\Delta_1+\Delta_2)}+1=0,\end{gathered} \tag{52}$$

where $\sigma_{k,l}^{\pm} = \frac{\varepsilon_k\zeta_l \pm \varepsilon_l\zeta_k}{\varepsilon_k\zeta_l}$ with $k = 1$ and $l = 2$, or $k = 2$ and $l = 1$, $\varepsilon_j = \varepsilon_j(\omega)$ and $\zeta_j = \zeta_j(\omega, \kappa)$ for $j = 1, 2$.

To solve the second system, we also denote the corresponding matrix of the system coefficients in the following manner:

$$K_2(\omega,\kappa) = \begin{pmatrix} e^{i\zeta_1\Delta_1} & e^{-i\zeta_1\Delta_1} & -e^{i\zeta_2\Delta_1} & -e^{-i\zeta_2\Delta_1} \\ e^{i\zeta_1\Delta_1} & -e^{-i\zeta_1\Delta_1} & -\frac{\mu_1}{\mu_2}\frac{\zeta_2}{\zeta_1}e^{i\zeta_2\Delta_1} & \frac{\mu_1}{\mu_2}\frac{\zeta_2}{\zeta_1}e^{-i\zeta_2\Delta_1} \\ 1 & 1 & -e^{i\zeta_2(\Delta_1+\Delta_2)}e^{-i\theta(\Delta_1+\Delta_2)} & -e^{-i\zeta_2(\Delta_1+\Delta_2)}e^{-i\theta(\Delta_1+\Delta_2)} \\ 1 & -1 & -\frac{\mu_1}{\mu_2}\frac{\zeta_2}{\zeta_1}e^{i\zeta_2(\Delta_1+\Delta_2)}e^{-i\theta(\Delta_1+\Delta_2)} & \frac{\mu_1}{\mu_2}\frac{\zeta_2}{\zeta_1}e^{-i\zeta_2(\Delta_1+\Delta_2)}e^{-i\theta(\Delta_1+\Delta_2)} \end{pmatrix},$$

where $\mu_j = \mu_j(\omega)$ and $\zeta_j = \zeta_j(\omega, \kappa)$ for $j = 1, 2$, and compare the det $K_2(\omega, \kappa)$ determinant to zero. Then, recalling $\varepsilon_1(\omega) = \mu_1(\omega)$ and $\varepsilon_2(\omega) = \mu_2(\omega)$, we obtain the relation, which is identical to equation (52). This means that we have the identical PBG structure for the TE and TM modes.

## 3. Numerical results and discussion

### 3.1. PBG structure

We use a numerical approach to study the PBG structure of the considered 1DPC. We search for $\omega$ and $\kappa$ values where the equality (52) holds true with any $\theta$ value that belongs to the $(0,\ 2\pi/\Delta)$ interval. In the first part of our numerical investigation, we fix the constants $\Delta_1 = \Delta_2 = 10\quad \eta\mathrm{m}^{-1}$, $\omega_0 = 30$ THz, $\Omega = 90$ THz, and intervals for $\omega$ values from 0-240 THz (then the $\omega/c$normalized frequency has values from 0-0.8$\times10^6$ m$^{-1}$) and for $\kappa$ values from 0-0.8 $\eta\mathrm{m}^{-1}$ (i.e., to 0.8$\times10^6$ m$^{-1}$).

In accordance with the investigation [23], the $\zeta_j(\omega, \kappa)$ value in equation (52) can be real or distinctly imaginary. If $\zeta_j(\omega, \kappa)$ is real then in the $j$-th layer the radiative regime is observed else the evanescent regime. Thus, we have four different areas for $(\omega, \kappa)$ values (Fig. 1).

The PBG structure is presented in Fig. 2 and Fig. 3. In areas with numbers 1 and 3 for $\omega < \omega_2$, where $\omega_2 = 94.86$ THz (Fig. 1) and the radiative regime for the metamaterial is observed (see Fig. 2 and (a)-(d) in Fig. 3), there are a set of permitted bands, which ones comprise one continuous band for $\kappa = 0$ and become narrower and converge to a linear bands with ncreased $\kappa$ values. Also, the permitted become narrower and more thickly located when $\omega$ approaches $\omega_0$. For the NIM and first PIM intervals we observe different PBG structures. Namely, with increased $\kappa$ values, the linear permitted bands are bent in the left side for the NIM interval and in the right side for the PIM interval (see (a)-(d) in Fig. 3 and Fig. 2, respectively).

In both areas marked number 4 (Fig. 1), there are no permitted bands, except the one band with $\omega$ values beside the $\omega_1 = 70.35$ THz NIM frequency (see (d) in Fig. 3). With increased $\kappa$ values, the permitted band becomes narrower and converges to the $\omega_1$ value, i.e., for the NIM frequency, there is no reflection effect for all $\kappa$ values. This fact was discussed for the finite periodic system, similar to that considered in [27], for the NIM single layer in

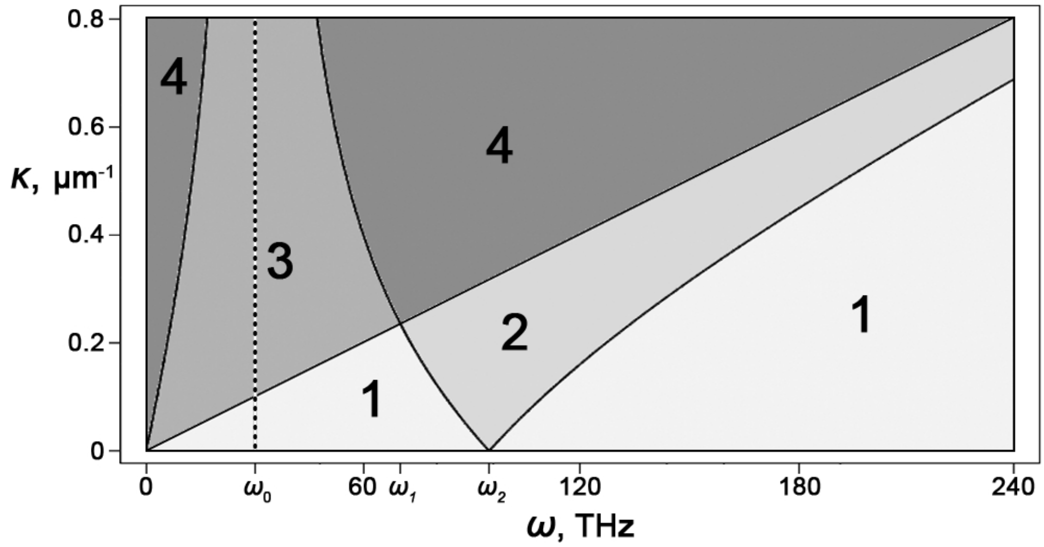


FIG. 1. Areas of the radiative and evanescent regimes. Black unbroken lines divide the $(\omega, \kappa)$ space into areas. Areas with number 1 correspond to cases when the radiative regime is observed in the metamaterial and vacuum simultaneously. Area number 2 corresponds to the case when the evanescent regime is observed in the metamaterial and the radiative regime is observed in the vacuum. Area number 3 corresponds to the case when the radiative regime is observed in the metamaterial and the evanescent regime is observed in the vacuum. Areas with number 4 correspond to the cases when the evanescent regime is observed in the metamaterial and vacuum simultaneously. The vertical dotted line corresponds to the $\omega_0 = 30$ THz frequency. $\omega_1 = 70.35$ THz is the NIM frequency, i.e., $\varepsilon_1(\omega_1) = \mu_1(\omega_1) = -1$. For the $\omega_2 = 94.86$ THz frequency $\varepsilon_1(\omega_2) = \mu_1(\omega_2) = 0$

vacuum [28], and for the system, composed of two half spaces filled with NIM and vacuum [23].

In the area with the number 1 for $\omega > \omega_2$ (see Fig. 1 and (e) in Fig. 3), there are no forbidden bands, except the narrow band that follows the boundary divided areas with numbers 1 and 2. The PBG structure of the second PIM interval is different from the ones for the first PIM and the NIM intervals (see (e) and (a)-(d) in Fig. 3 and Fig. 2, respectively).

The area with the number 2 (Fig. 1) has only two permitted bands. The first one arises at $\omega_2$ and follows the boundary divided areas with numbers 2 and 4 (see (e) in Fig. 3). The second permitted band is located near the $\omega_1$ NIM frequency (see (d) in Fig. 3).

### 3.2. Modification of Lorentz contribution parameters

Now, we examine the band gap structure of the considered system for the different values of $\omega_0$ and $\Omega$. We consider the following cases:

A) $\omega_0 = 30$ THz and $\Omega = 30$ THz
B) $\omega_0 = 30$ THz and $\Omega = 60$ THz
C) $\omega_0 = 60$ THz and $\Omega = 30$ THz
D) $\omega_0 = 30$ THz and $\Omega = 75$ THz
E) $\omega_0 = 75$ THz and $\Omega = 30$ THz

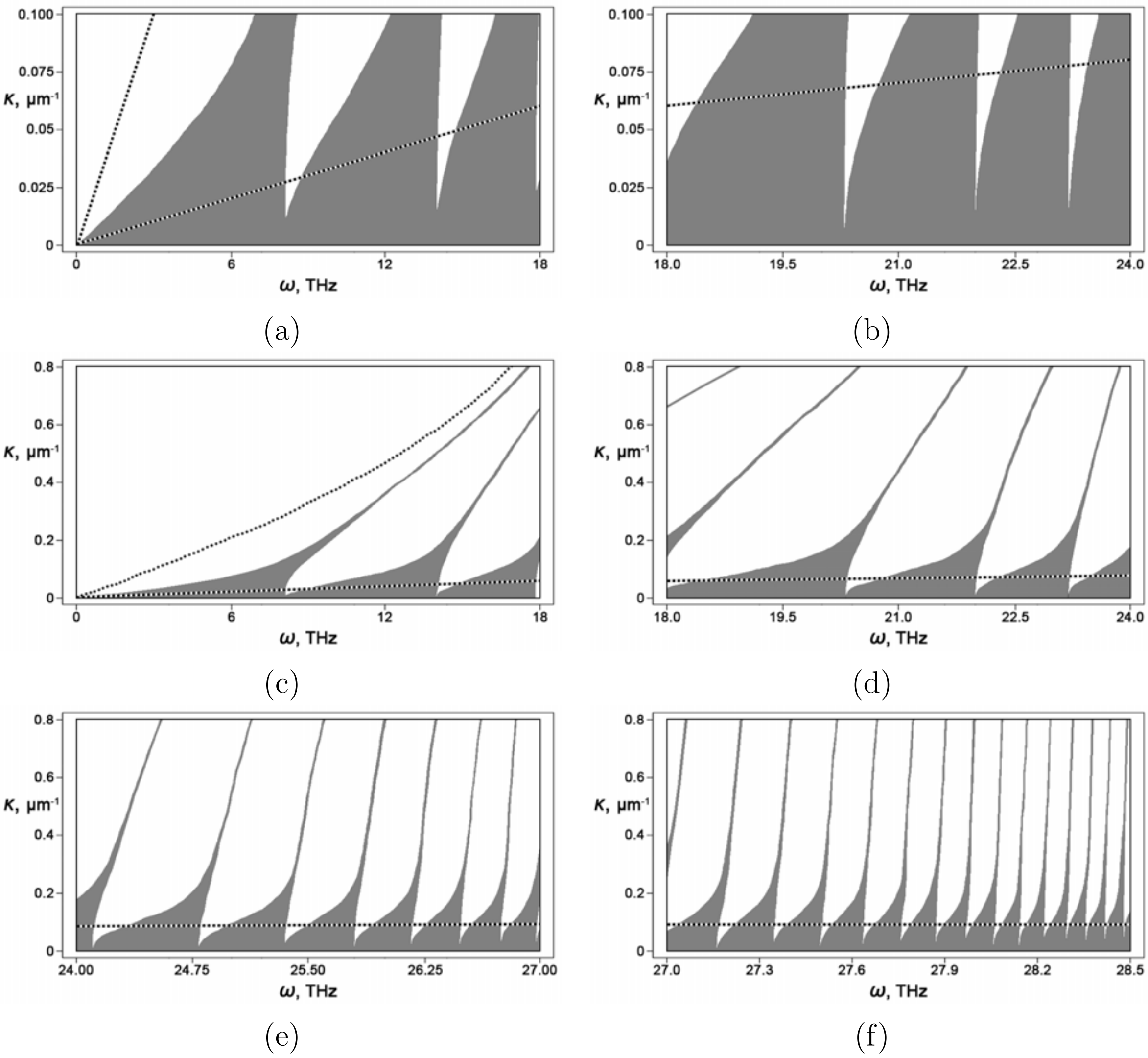


FIG. 2. Dependences of PBG structure on the $\omega$ frequency and $\kappa$ values for TE and TM mode simultaneously. Permitted bands are gray, forbidden bands are white. Dotted lines divide the $(\omega, \kappa)$ space into four different areas (see Fig. 1). The metamaterial behaves like PIM

The D and E cases are as additional ones. We fix the constants $\Delta_1 = \Delta_2 = 10 \quad \eta\mathrm{m}^{-1}$ and the intervals for $\omega$ values from 0-90 THz (then the $\omega/c$normalized frequency has values from 0-0.3$\times 10^6$ m$^{-1}$) and for $\kappa$ values from 0-0.3 $\eta$m$^{-1}$ (i.e., to 0.3$\times 10^6$ m$^{-1}$). As we noted above, $(\omega, \kappa)$ values comprise four different areas (Fig. 4).

Let us consider the doubling of the $\Omega$ constant, i.e., the A and B cases. It brings to a broadening of the radiative regime area for the metamaterial layers. The $\omega_2$ value increases from 42.42 to 67.08 THz and the NIM interval of the $\omega$ frequency becomes wider but the first PIM interval of the $\omega$ frequency remains unchanged (see (a) and (b) in Fig. 4). The permitted bands become narrower and more thickly located (see (a) and (b) in Fig. 5). The permitted band, which contains the NIM frequency, redoubles along the $\omega$ axis (see (d) and (e) in Fig. 5). For the A, B and D cases we consider the $\omega$ frequency intervals of the same 24 THz length with the beginning in $\omega_2$ (see (a), (b), and (c) in Fig. 6). With increasing of the $\Omega$ constant, the permitted band in the 2 area (Fig. 4) becomes narrower and the adjacent

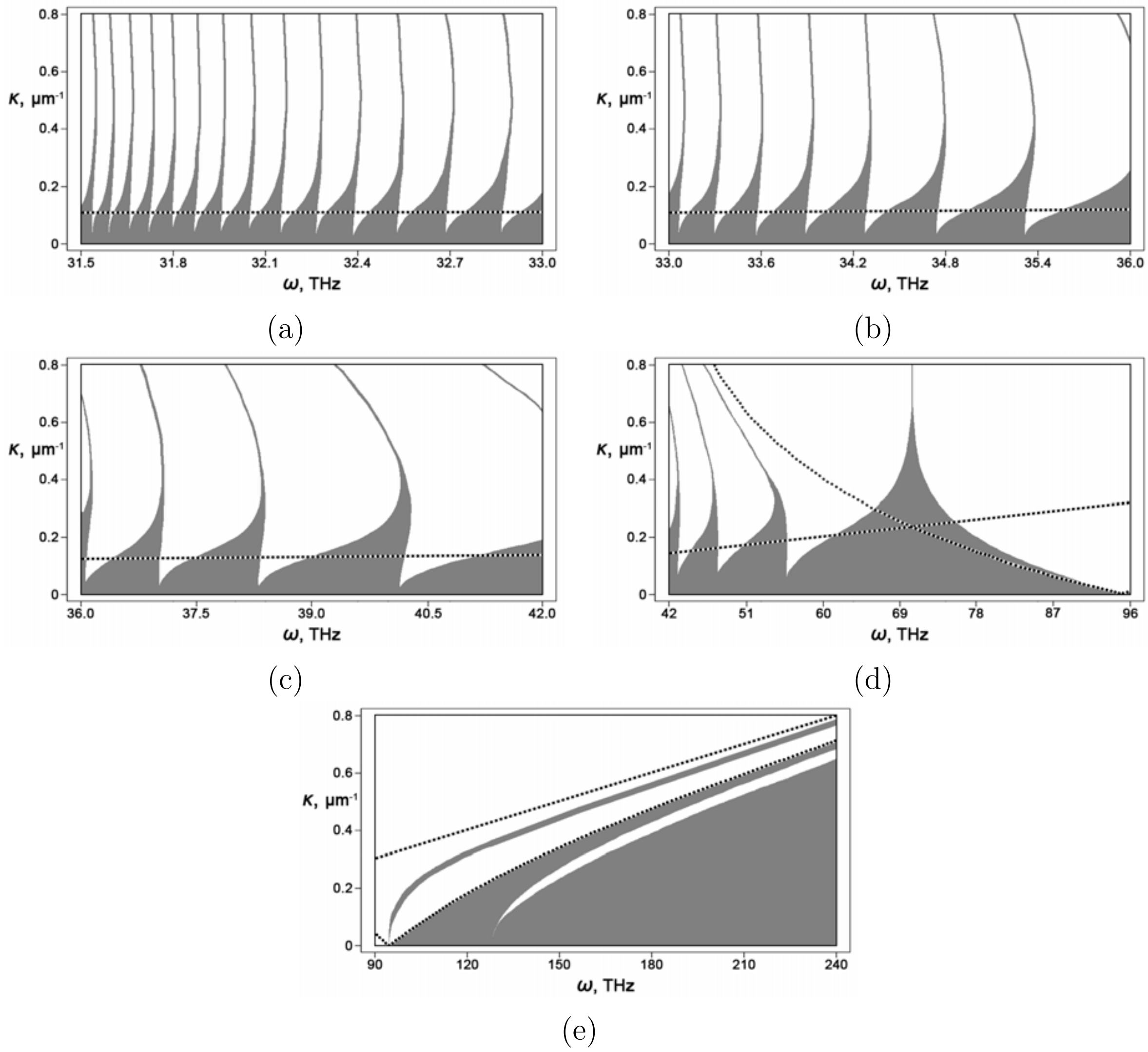


FIG. 3. Dependences of PBG structure on the $\omega$ frequency and $\kappa$ values for TE and TM mode simultaneously. Permitted bands are grey, forbidden bands are white. Dotted lines divide the $(\omega, \kappa)$ space into four different areas (see Fig. 1). The metamaterial behaves like NIM (a)-(d), and PIM (e)

permitted band grows to the whole second part of the 1 area (Fig. 4). The forbidden band between these permitted bands becomes wider along the $\kappa$ axis.

Now, we consider the doubling of the $\omega_0$ constant, i.e., the A and C cases. As for the A and B cases, it elicits a broadening of radiative regime area for the metamaterial layers. The $\omega_2$ value also increases from 42.42 to 67.08 THz, but the NIM interval of the $\omega$ frequency becomes narrower and the PIM interval of the $\omega$ frequency becomes wider (see (a) and (c) in Fig. 4). With increased $\kappa$ values, the permitted bands become narrower but not as quickly as in the A case. The permitted band, which contains the NIM frequency, have lost about half of its width along the $\omega$ axis (see (d) and (f) in Fig. 5). Analogously, with the A, B and D cases, for the A, C and E cases we consider the $\omega$ frequency intervals of the same 24 THz length with the beginning in $\omega_2$ (see (a), (d), and (e) in Fig. 6). With increasing of the $\omega_0$ constant, the permitted band in the 2 area (Fig. 4) becomes narrower. It seems that

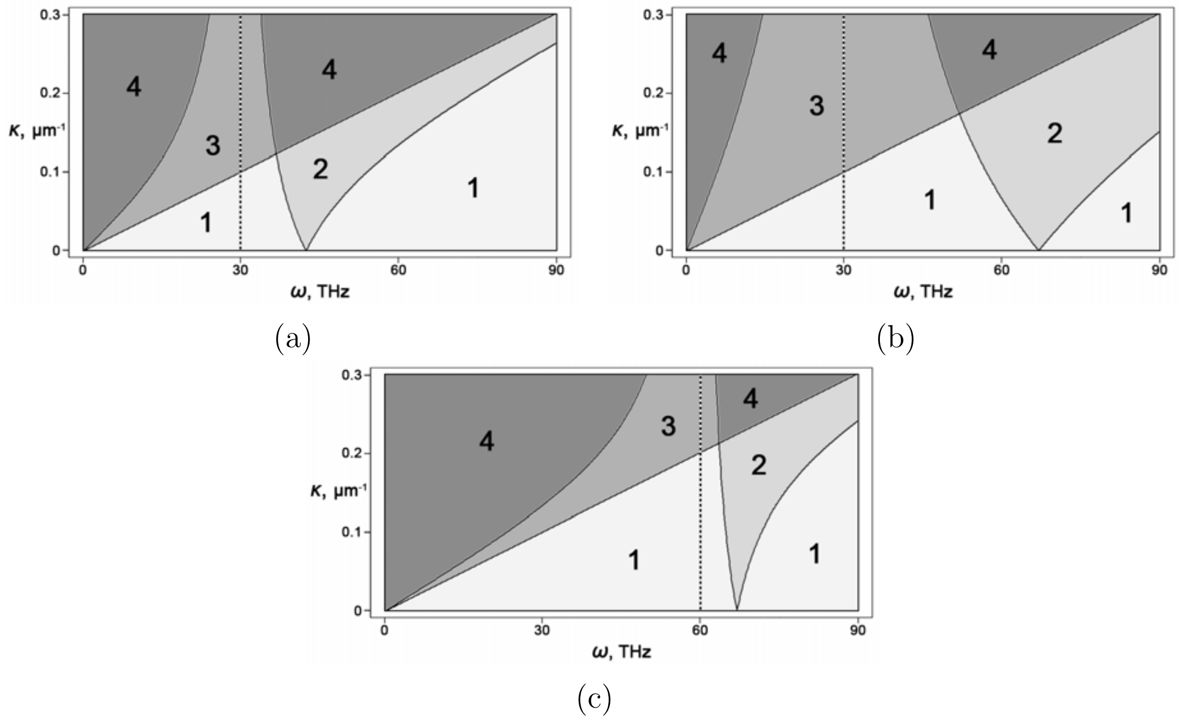


FIG. 4. Areas of the radiative and evanescent regimes. Black unbroken lines divide the $(\omega, \kappa)$ space into areas. Areas with number 1 correspond to the cases when the radiative regime is observed in the metamaterial and vacuum simultaneously. Area number 2 corresponds to the case when the evanescent regime is observed in the metamaterial and the radiative regime is observed in the vacuum. Area number 3 corresponds to the case when the radiative regime is observed in the metamaterial and the evanescent regime is observed in the vacuum. Areas with number 4 correspond to the cases when the evanescent regime is observed in the metamaterial and vacuum simultaneously. The vertical dotted line corresponds to the $\omega_0$ frequency. The A, B, and C cases are presented in (a), (b), and (c), respectively

the forbidden band located between that permitted and the next band remains unchanged in width along the $\kappa$ axis.

### 3.3. Modification of layer's width

The third our numerical investigation consists in changing of the $\Delta_1$ and $\Delta_2$ parameters. We fix $\omega_0 = 30$ THz, $\Omega = 90$ THz and use the four following combinations:

*a*) $\Delta_1 = \Delta_2 = 10 \quad \eta$m (see (a) in Fig. 7-10)
*b*) $\Delta_1 = 20 \quad \eta$m and $\Delta_2 = 10 \quad \eta$m (see (b) in Fig. 7-10)
*c*) $\Delta_1 = 10 \quad \eta$m and $\Delta_2 = 20 \quad \eta$m (see (c) in Fig. 7-10)
*d*) $\Delta_1 = 10 \quad \eta$m and $\Delta_2 = 100 \quad \eta$m (see (d) in Fig. 7-10 and (e) in Fig. 8)

With the each combination, we obtain the PBG structure of the considered system for different $\omega$ frequencies:

1) from 0 till 18 THz (Fig. 7)
2) from 36 till 42 THz (Fig. 8)
3) from 42 till 96 THz (Fig. 9)
4) from 90 till 120 THz (Fig. 10)

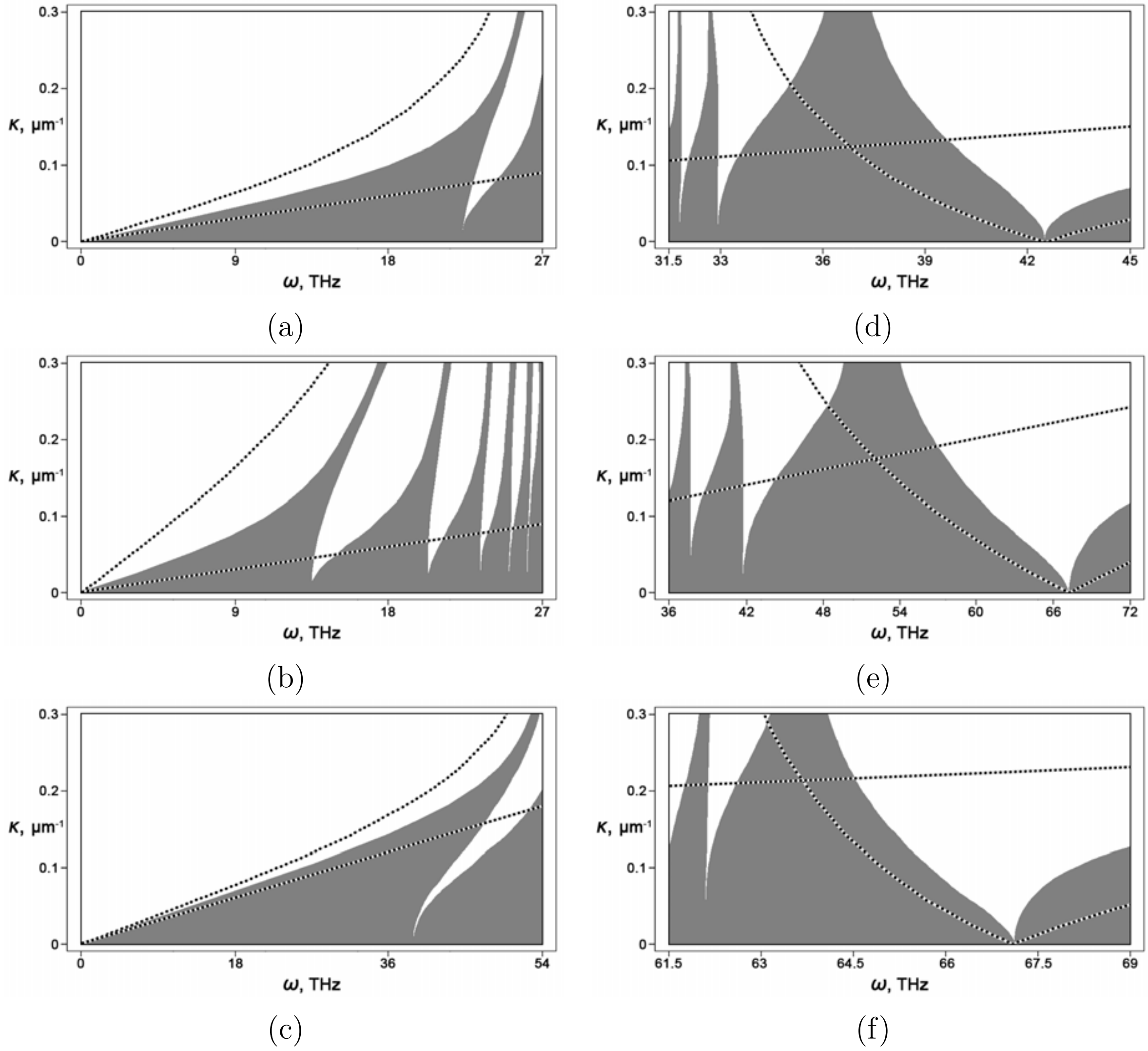


Fig. 5. Dependences of PBG structure on the $\omega$ frequency and $\kappa$ values for TE and TM mode simultaneously. Permitted bands are grey, forbidden bands are white. Dot lines divide the $(\omega, \kappa)$ space on four different areas (see Fig. 4). The A case is presented in (a) and (d). The B case is presented in (b) and (e). The C case is presented in (c) and (f)

We obtain that doubling of the $\Delta_1$ parameter (the $a$ and $b$ combinations) results in the approximately two-fold narrowing of the permitted and forbidden bands simultaneously (see (a) and (b) in Fig. 7-10). The permitted band, which contains the NIM frequency, is split into two bands (see and (b) in Fig. 9). There is no more absence of reflection for the NIM frequency, which is observed with the $a$ combination (see (a) in Fig. 9).

Increasing of the $\Delta_2$ parameter ($a$, $c$, and $d$ combinations) results in a faster narrowing of the permitted bands with increased $\kappa$ values (see (c) and (d) in Fig. 7-10), than is observed for the $a$ combination (see (a) in Fig. 7-10). It seems that the permitted bands for small $\kappa$ values become narrower and shift to the zero $\omega$ value. Also, for the $d$ combination we observe conglutination of adjacent permitted bands (see (d) in Fig. 7 and (d) and (e) in Fig. 8). The right 1 area and the 2 area (Fig. 1) are filled with narrow linear permitted bands, which ones are bent approximately parallel to the bound between areas 1 and 2 (see (d) in Fig. 10).

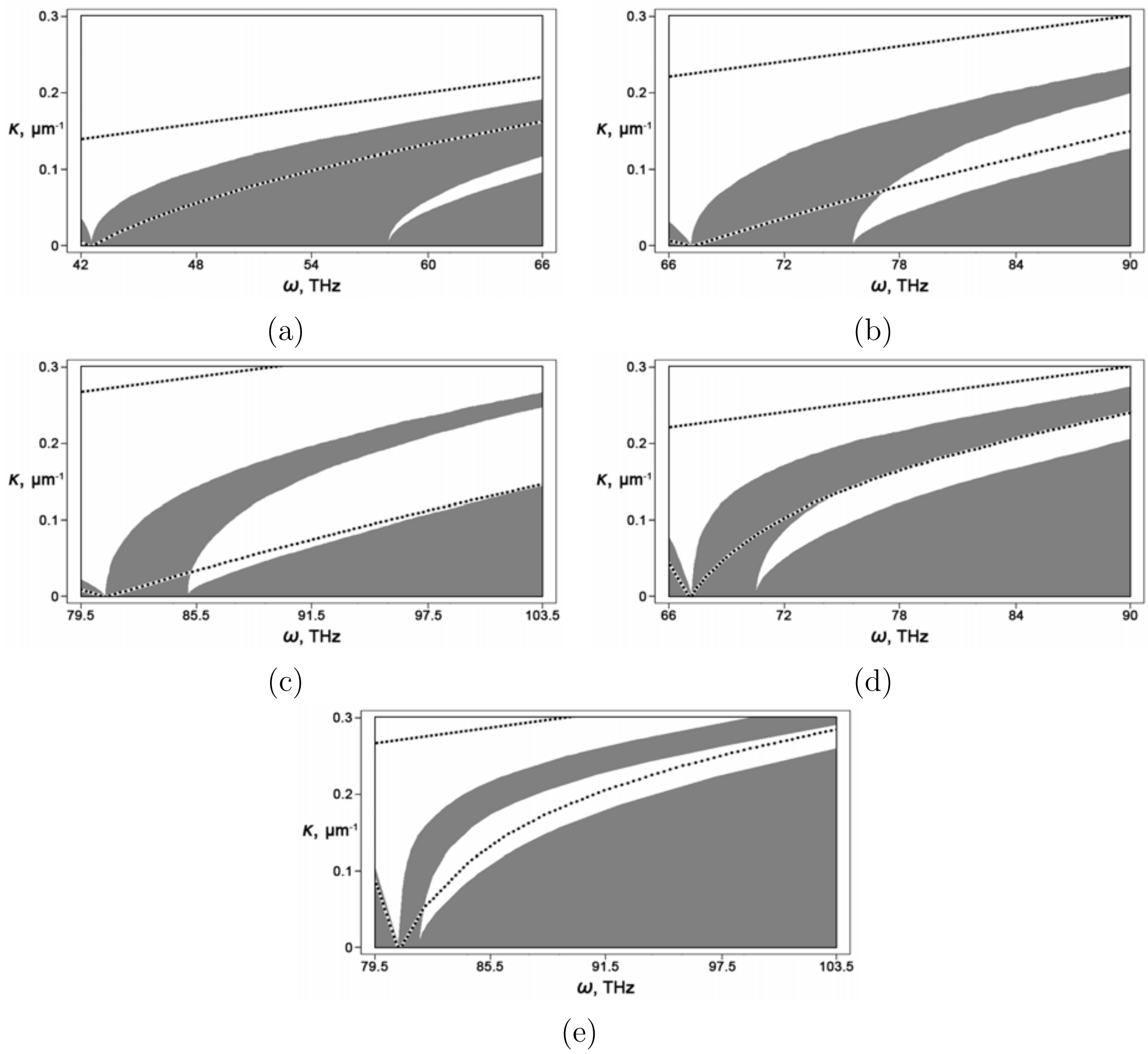


Fig. 6. Dependences of PBG structure on the $\omega$ frequency and $\kappa$ values for TE and TM mode simultaneously. Permitted bands are gray, forbidden bands are white. Dotted lines divide the $(\omega, \kappa)$ space into four different areas (see Fig. 4). The A, B, C, D, and E cases are presented in (a), (b), (c), (d), and (e), respectively

The permitted band, which contains the NIM frequency, is split into two bands (see (c) and (d) in Fig. 9). As with the $b$ combination, there is no more absence of reflection for the NIM frequency, which is observed with the $a$ combination (see (a) in Fig. 9).

## 4. Conclusions

In this paper, we solved the problem of obtaining the PBG structure for a system composed of an infinite number of alternating parallel layers filled with a metamaterial and vacuum, i.e., for the 1DPC. We assumed the Fourier transformed permittivity and permeability stood equal and were expressed through a singly dispersive Lorentz term (16). This produced identical PBG structures for TE and TM modes. We considered combinations for the radiative and evanescent regimes in metamaterial and vacuum layers.

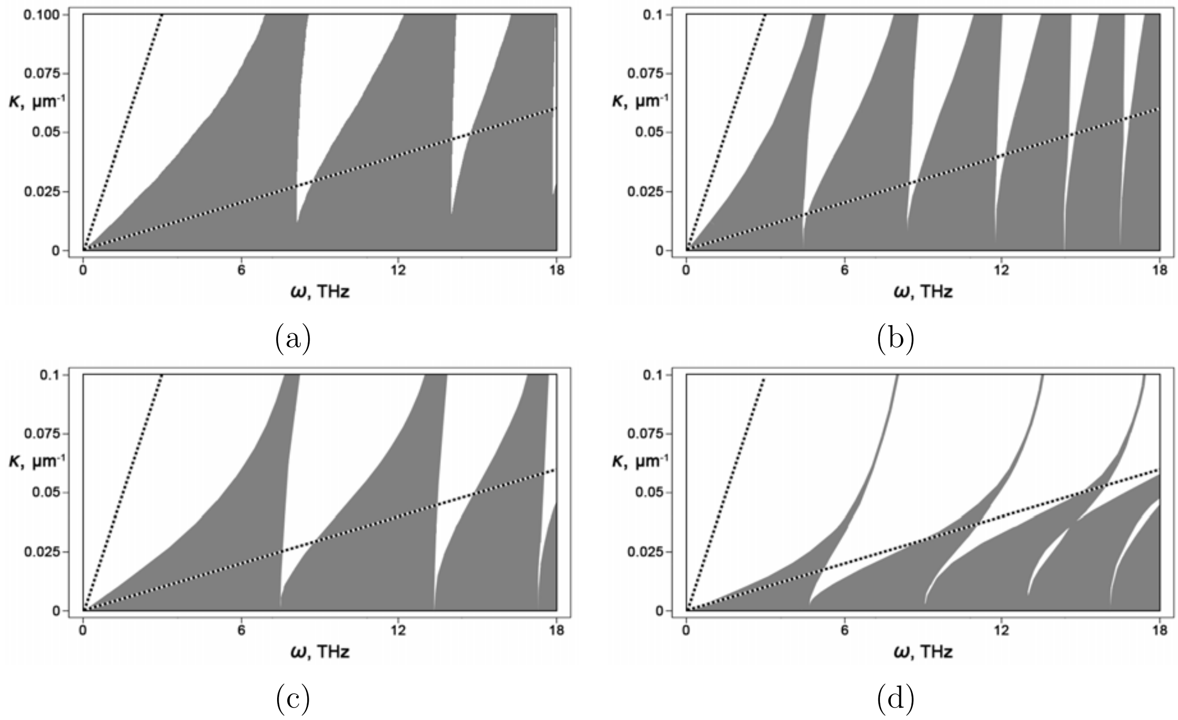


Fig. 7. Dependences of PBG structure on the $\omega$ frequency and $\kappa$ values for TE and TM mode simultaneously. Permitted bands are gray, forbidden bands are white. Dotted lines divide the $(\omega, \kappa)$ space into four different areas (Fig. 1). The $a$, $b$, $c$, and $d$ combinations are presented in (a), (b), (c), and (d), respectively

We obtained that for the radiative regime in metamaterial layers and both regimes in vacuum layers, there is a set of forbidden and permitted bands, ones which become narrower with the tending of the $\omega$ frequency to approach the $\omega_0$ constant of the single Lorentz term expression (16). For the $\omega$ frequency intervals, where the metamaterial behaves like the NIM or PIM, we observe the different PBG structures. For the NIM frequency we observe the no reflection effect for any directions. This fact was discussed earlier for finite layered systems [23, 27, 28].

With an increase in the $\Omega$ parameter, we observed the increasing of the $\omega$ frequency interval, where the metamaterial behaves like NIM. The PBG structure became wider. With an increase in the $\omega_0$ parameter, we observed a widening of the $\omega$ frequency interval, where the metamaterial behaves like a PIM, but for decreasing values, the metamaterial behaves like a NIM. The PBG structure became more extended along the $\kappa$ axis.

With increased $\Delta_1$ metamaterial layer width, the PBG structure became wider. With increased $\Delta_2$ vacuum layer width, the permitted bands were accumulated in the $(\omega, \kappa)$ area, where the radiative regime for the metamaterial and vacuum is observed simultaneously. For other $(\omega, \kappa)$ areas, the permitted bands converged to the lines. In both cases (grow of $\Delta_1$ or $\Delta_2$) the permitted band contained the NIM frequency was split into two bands, i.e., there is no more absence of reflection for the NIM frequency, which was observed earlier. This fact disagrees with results for finite layered systems [23, 27, 28] and thus, is cause for increased interest.

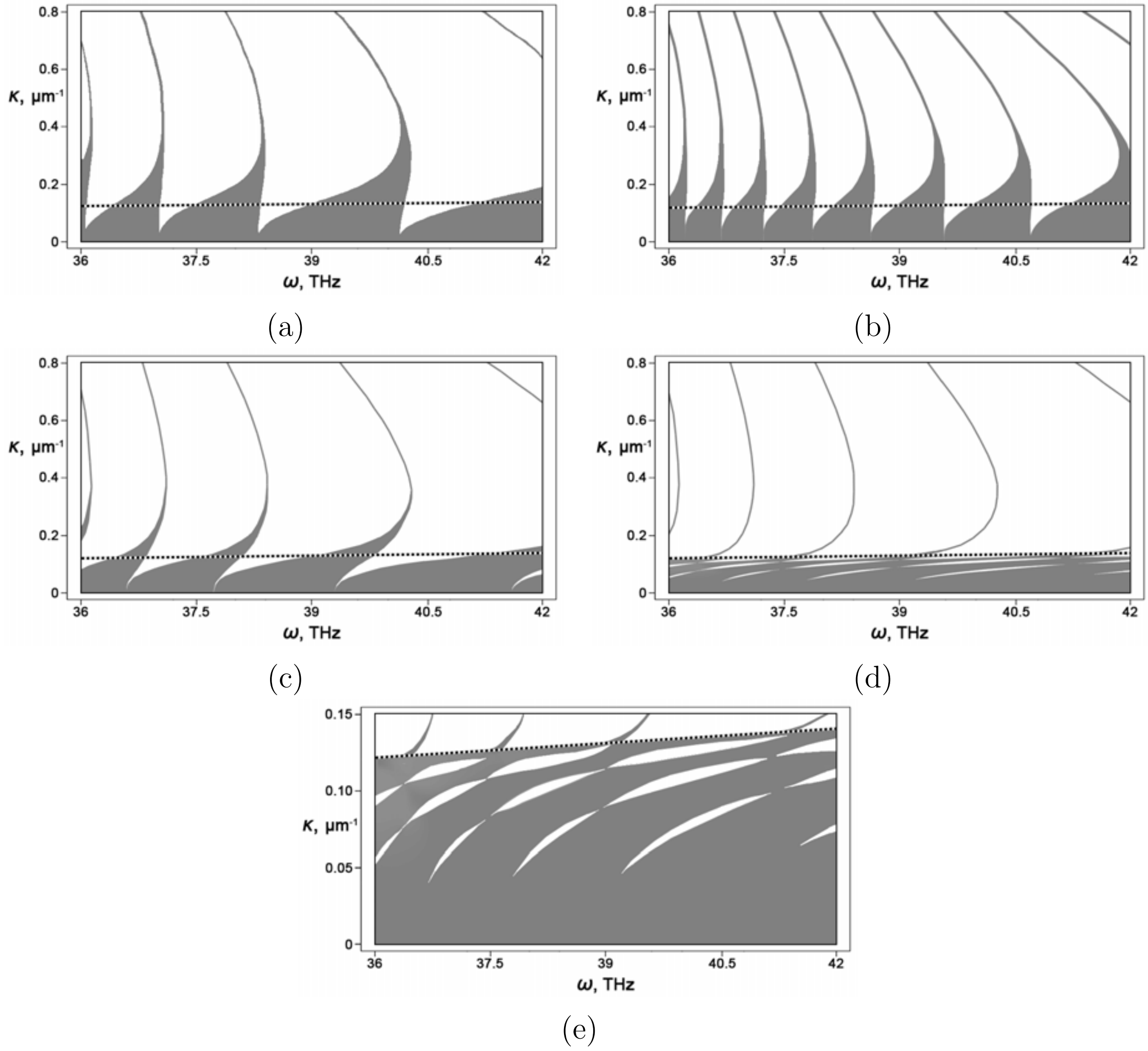


FIG. 8. Dependences of PBG structure on the $\omega$ frequency and $\kappa$ values for TE and TM mode simultaneously. Permitted bands are gray, forbidden bands are white. Dotted lines divide the $(\omega, \kappa)$ space into four different areas (Fig. 1). The $a$, $b$, $c$, and $d$ combinations are presented in (a), (b), (c), and (d), respectively

**Acknowledgments**

The work was partially financially supported by the Government of the Russian Federation (Grant 074-U01), by State contract of the Russian Ministry of Education and Science and grants of the President of Russia (state contract 14.124.13.2045-MK and grant MK-1493.2013.1).

## References

[1] P. Vukusic, J.R. Sambles. Photonic structures in biology. *Nature*, **424**, P. 852–855 (2003).
[2] E. Yablonovitch. Inhibited Spontaneous Emission in Solid-State Physics and Electronics. *Phys. Rev. Lett.*, **58**, P. 2059–2062 (1987).
[3] S. John. Strong localization of photons in certain disordered dielectric superlattices. *Phys. Rev. Lett.* **58**, P. 2486–2489 (1987).

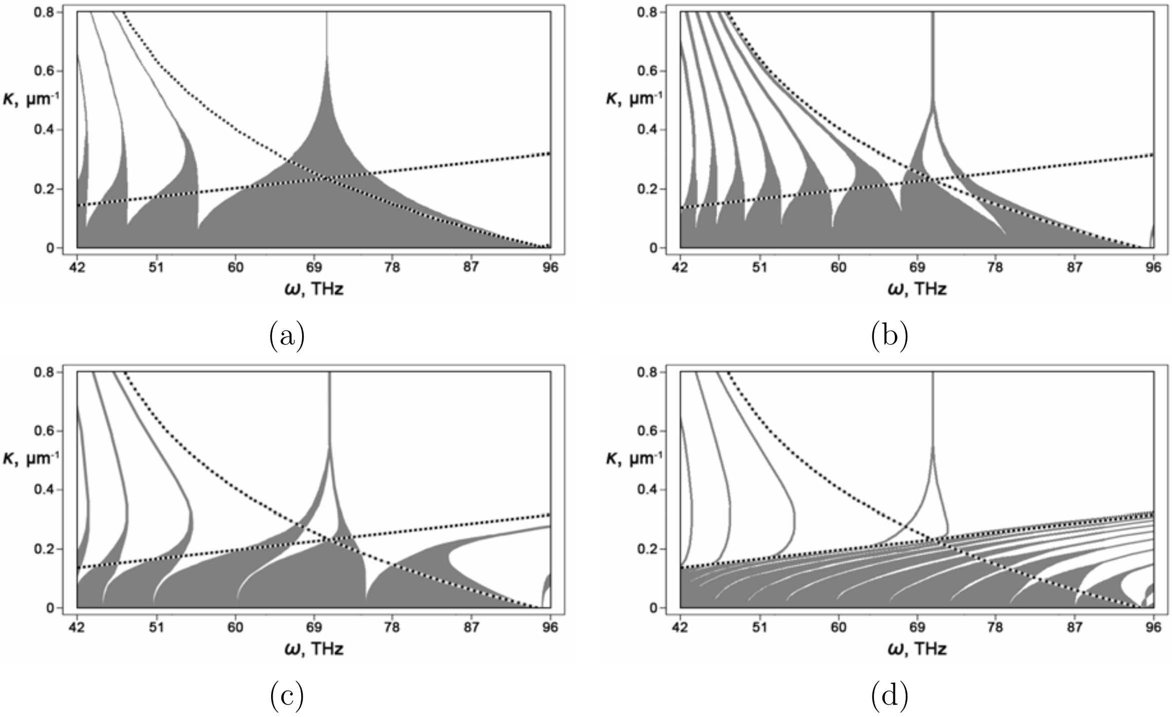


FIG. 9. Dependences of PBG structure on the $\omega$ frequency and $\kappa$ values for TE and TM mode simultaneously. Permitted bands are gray, forbidden bands are white. Dotted lines divide the $(\omega, \kappa)$ space into four different areas (Fig. 1). The $a$, $b$, $c$, and $d$ combinations are presented in (a), (b), (c), and (d), respectively


[4] J.D. Joannopoulos, S.G. Johnson, J.N. Winn, R.D. Meade. *Photonic Crystals: Molding the Flow of Light.* Princeton University Press, Princeton, second edition, 286 p. (2008).

[5] K. Sakuda. *Optical Properties of Photonic Crystals.* Springer-Verlag, Berlin, second edition, 253 p. (2005).

[6] Y. Fink, J.N. Winn, S. Fan, J. Michel, C. Chen, J.D. Joannopoulos, E.L. Thomas. A dielectric omnidirectional reflector. *Science*, **282**, P. 1679–1682 (1998).

[7] J.M. Dudley, J.R. Taylor. Ten years of nonlinear optics in photonic crystal fibre. *Nat. Phot.*, **3**, P. 85–90 (2009).

[8] J. Rosenberg, R.V. Shenoi, S. Krishna, O. Painter. Design of plasmonic photonic crystal resonant cavities for polarization sensitive infrared photodetectors. *Opt. Exp.*, **18**, P. 3672–3686 (2010).

[9] A.M.R. Pinto, M. Lopez-Amo. Photonic Crystal Fibers for Sensing Applications. *Journal of Sensors*, **2012**, P. 598178-21 (2012).

[10] A.C. Liapis, Z. Shi, R.W. Boyd. Optimizing photonic crystal waveguides for on-chip spectroscopic applications. *Opt. Exp.*, **21**, P. 10160–10165 (2013).

[11] H. Altug. *PhD Dissertation*, Stanford University, Stanford, 120 p. (2006).

[12] V.G. Veselago. The electrodynamics of substances with simultaneously negative values of $\varepsilon$ and $\mu$. *Sov. Phys. Usp.*, **10**, P. 509–514 (1968).

[13] J.B. Pendry. Negative Refraction Makes a Perfect Lens. *Phys. Rev. Lett.*, **85**, P. 3966–3969 (2000).

[14] L. Wu, S. He, L. Shen. Band structure for a one-dimensional photonic crystal containing left handed materials. *Phys. Rev. B*, **67**, P. 235103–10 (2003).

[15] H. Jiang, H. Chen, H. Li, Y. Zhang, J. Zi, S. Zhu. Properties of one dimensional photonic crystals containing single-negative materials. *Phys. Rev. E*, **69**, P. 066607-10 (2004).

[16] D. Bria, B. Djafari-Rouhani, A. Akjouj, L. Dobrzynski, J.P. Vigneron, E.H. El Boudouti, A. Nougaoui. Band structure and omni directional photonic band gaps in lamellar structure with left handed materials. *Phys. Rev. E*, **69**, P. 066613-12 (2005).

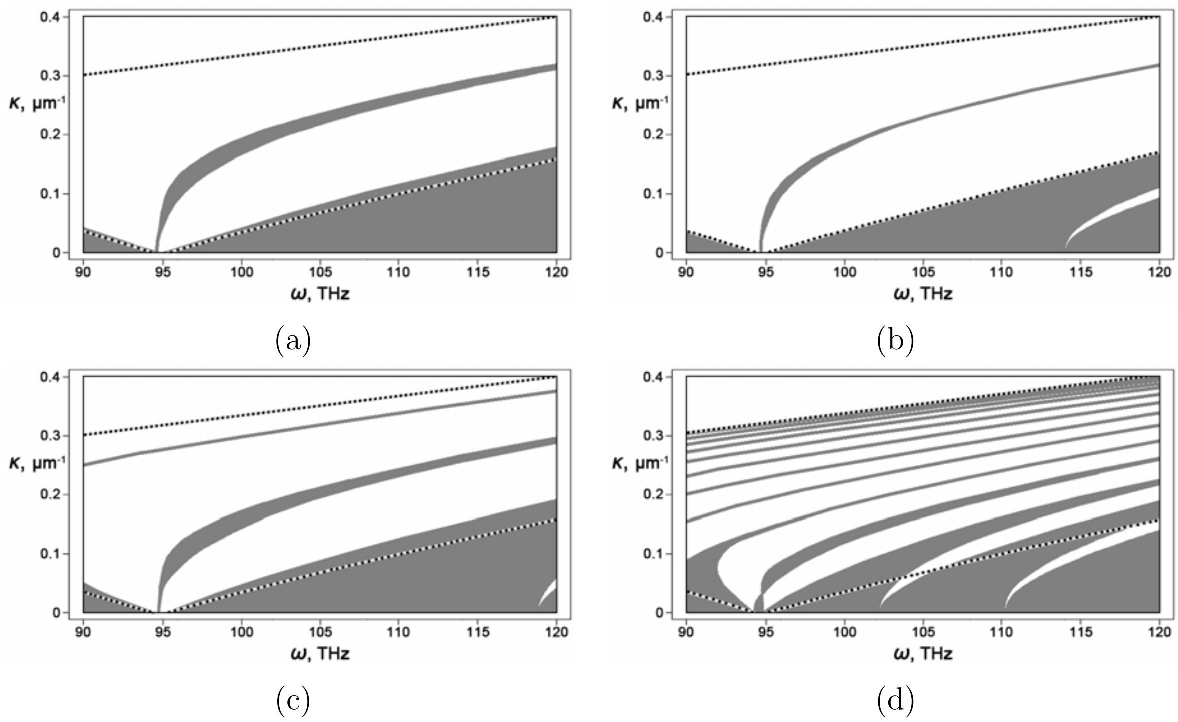


Fig. 10. Dependences of PBG structure on the $\omega$ frequency and $\kappa$ values for TE and TM mode simultaneously. Permitted bands are gray, forbidden bands are white. Dotted lines divide the $(\omega, \kappa)$ space into four different areas (Fig. 1). The $a$, $b$, $c$, and $d$ combinations are presented in (a), (b), (c), and (d), respectively

[17] S. K. Singh, J.P. Pandey, K.B. Thapa, S.P. Ojha. Structural parameters in the formation of omnidirectional high reflectors. *PIER*, **70**, P. 53–78 (2007).

[18] C. Nicolae, R.M. Osgood, Jr.S. Zhang, S.R.T. Brueck. Zero-n bandgap in photonic crystal superlattices. *J. Opt. Soc. Am. B*, **23**, P. 506–512 (2006).

[19] H. Jiang, H. Chen, S. Zhu. Localized gap-edge fields of one-dimensional photonic crystals with an $\varepsilon$-negative and a $\mu$-negative defect. *Phys. Rev. E*, **79**, P. 0466601-8 (2006).

[20] G.N. Pandey, K.B. Thapa, S.K. Srivastava, S.P. Ojha. Band structures and abnormal behavior of one dimensional photonic crystal containing negative index materials. *PIER M*, **2**, P. 15–36 (2008).

[21] X. Feng, H. Li. Enlargement of the omnidirectional reflectance gap in one-dimensional photonic crystal heterostructure containing double negative index material. *Eur. Phys. J. D*, **67**, P. 40157-7 (2013).

[22] A. Tip. Linear dispersive dielectrics as limits of Drude-Lorentz systems. *Phys. Rev. E*, **69**, P. 016610-5 (2004).

[23] B. Gralak, A. Tip. Macroscopic Maxwell's equations and negative index materials. *J. Math. Phys.*, **51**, P. 052902-28 (2010).

[24] G. Floquet. Sur les équations différentielles linéaires á coefficients périodiques. *Ann. Ecole Norm. Sup.*, **12**, P. 47–88 (1883).

[25] F. Bloch. Über die Quantenmechanik der Elektronen in Kristallgittern. *Z. Phys.*, **52**, P. 555–600 (1929).

[26] L. Novotny, B. Hecht. *Principles of Nano-Optics*. Cambridge University Press, New York, 539 p. (2006).

[27] K. Pravdin, I. Popov. Point source in the layered medium with metamaterials: method of recurrent relations. *Sc. Tech. J. Inf. Tech. Mech. Opt.*, **91**, P. 11–17 (2014).

[28] K.V. Pravdin, I.Yu. Popov. Model of the interaction of point source electromagnetic fields with metamaterials. *Nanosystems: Phys. Chem. Math.*, **4**, P. 570–576 (2013).